APPLICATION OF SINGLE OBJECTIVE GENETIC ALGORITHM TO OPTIMIZE HEAT TRANSFER ENHANCEMENT FROM A FLAT PLATE

M. Kahrom [*] ***and S. M. Javadi***

Mechanical Engineering Department, Ferdowsi University of Mashhad, Mashhad, Iran
Mohsen.kahrom@yahoo.co.uk, mohammad.javadi@gmail.com

*Corresponding Author

(Received: November 11, 2010 – Accepted in Revised Form: December 15, 2011)

doi: *10.5829/idosi.ije.2012.25.01c.08*

Abstract Prior numerical investigations show that, if an object is placed into a turbulent boundary layer, it affects on near wall flow structure, alters heat transfer and friction coefficient of the nearby wall. To govern these flow features, a quadrilateral insert is selected as a promoter. The frontal face of the quad acts to control the size and position of the upstream stagnation point. The face parallel to the wall controls the formation and development of near wall jet and two other faces operate in controlling the rearward circulation zone. Having these all faces set, the heat transfer optimization of the neighboring flat plate is left to examination. The quad is inserted into the boundary layer while its shape and distance from the flat plate is repeatedly modified to gain moderate forms of disruption and improvement in heat transfer coefficient. The single objective Genetic Algorithm (GA) as a tool, coupled with the modified Teach-t code was employed to optimize the shape and distance of the obstacle from the plate. When application of optimal geometry is reached, the mean heat transfer coefficient over the affected area of the flat plate was enhanced by more than 51%. The study of flow features around the quad show that; each feature makes its own contribution to the heat transfer change from the flat plate. Common to all cases under study, the frontal stagnation point formed on the quad, counts for the slight decrease in the heat transfer coefficient, while the jet underneath the obstacle followed by the developing boundary layer are responsible for the sudden increase of the heat transfer coefficient. However, the downstream circulating flow area makes the main and widespread contribution.

Keywords Heat Transfer Enhancement; Optimization; Genetic Algorithm; Quadrilateral Insert; Turbulent Boundary Layer.

چکیده مطالعات گذشته نشان داده اند که اگر یک جسم در داخل لایه مرزی توربولنت قرار گیرد بر ساختار جریان در کنار دیواره تاثیر می گذارد و ضریب انتقال حرارت و اصطکاک را تغییر می دهد. برای مطالعه تاثیر شکل جسم بر ساختار لایه مرزی، یک جسم چهارگوش در داخل لایه مرزی در نظر گرفته شده است. در سطح رو–در–روی جریان، یک نقطه سکون تشکیل می شود و اندازه سطح کنترل کننده موقعیت و فشار نقطه سکون است. ضلع دیگر چهار گوش که موازی دیواره تخت است یک جت تشکیل می دهد و کنترل کننده عرض و سرعت جت است. بالاخره دو ضلع دیگر کنترل کننده اندازه و موقعیت پس‌گرده از جسم هستند. با کنترل اضلاع این چارگوش ساختار جریان در کنار دیواره تغییر می کند و اثر آن بر روی ضریب انتقال حرارت و ضریب اصطکاک مورد بحث و بررسی قرار گرفته است. اضافه بر این فاصله چهارگوش از صفحه تخت نیز بر شکل لایه مرزی تاثیر گذار است. با قرار دادن چنین چهارگوشی در فواصل مختلف از صفحه تخت و تغییر موقعیت اضلاع آن و با کمک الگوریتم ژنتیک شکل و ابعاد چهارگوش بهینه شده است. نتایج نشان می دهند که ورود چهار گوش بهینه به داخل لایه مرزی ضریب انتقال حرارت روی صفحه تخت را تا ۵۱٪ افزایش می دهد.

1. INTRODUCTION

In most industrial flows, only a narrow portion of the near wall velocity profile is seriously deformed due to the action of viscosity. It is called the boundary layer. Along with this short distance from the wall, the velocity and the temperature profile change sharply to attain their values in main

Nomenclature

A, B, C and D	Four corners of the quadrilateral obstacle
c_p	Specific heat
E	Total energy
C_μ, σ_k, σ_ε, $C_{1\varepsilon}$, $C_{2\varepsilon}$	Constants of $\kappa-\varepsilon$ equation, as defined in the text
$h_{c,x}$, $\overline{h_c}$	local and averaged Heat transfer coefficient
k	Conduction heat transfer coefficient
p	Static pressure
q''	Heat flux
S	Mesh expansion factor
T	Temperature
U	Main stream flow velocity
x, y	Longitudinal and transversal coordinates, respectively
t	time

Greek Symbols

μ	Dynamic viscosity
ρ	Mass density
δ_v	Velocity boundary layer thickness
δ_t	Thermal boundary layer thickness
τ	Shear stress
κ	Turbulent kinetic energy
λ_{eff}	$=\lambda+\lambda_t$, (molecular, plus turbulent thermal conductivity)

Abbreviation

RANS	RANS
SST	SST
LES	LES
DES	DES
RSM	RSM
LRN	LRN
HTC	Heat transfer coefficient
GA	Genetic Algorithm
Re	Reynolds number
y^+	Wall coordinates , y/δ_v
u^+	Wall coordinate, $\overline{u}/u_\tau$

Subscripts

i	x-wise properties of the nodes
j	y-wise properties of the nodes

Exponents

$-$	Average value of a parameter
'	Fluctuation component of a parameter

stream. Yet again, in the boundary layer, the most contribution in deformation of these profiles happens only at the first few percent of the boundary layer thickness close to the wall. In this very thin portion of the boundary layer, the flow structure and its features have vital effect on both heat transfer and friction coefficients.

Methods affecting the velocity profile are extensively used in last decades to modify the skin friction and delay the separation. Some have successfully put in industrial applications. Suction and blowing are conventional techniques in disruption of boundary layer profiles and are commonly used to whittle down the friction coefficient in fluid machineries, [1]. In addition, other passive and active methods including the polymer injection into the flow field, surface roughening, applications of dimples and penetration of main flow turbulence into the boundary layer are other techniques under consideration [2].

Amongst many extensive works and variety techniques that are employed for drag reduction of fluid flows, only a few techniques are extended to enhance the heat transfer from a wall. Noticeable amount of research has been conducted to shed light on the effects of free stream turbulence on heat transfer enhancement [3, 4]. Experimental studies of the effects of a cylindrical insert located above a flat plate and normal to a flow were treated by Kawaguchi et al. and also by Marumo et al. [5]. Kawaguchi [6] has experimentally studied the thermal characteristics of a flow disturbed by an array of cylinders which are mounted inside a boundary layer and parallel to the flow over a plate. Variety of traversal distances from the wall was considered. The results indicated some improvement of about 40% for heat transfer. While

the heat transfer enhancement was the main objective of the study for turbulent boundaries disturbed by a cylinder, dissimilarity between heat and momentum transfer was experimentally maintained by Suzuki et al. [7] and Souza [8]. Inaoka et al. [9] considered a square rod above a flat plate and numerically determined the existing dissimilarity and results are validated by experiments.

Similar study on heat transfer enhancement was conducted by insertion of a square rod into a forced convection turbulent boundary layer [10]. The numerical solution explores some features of flow around the obstacle that is difficult to conclude by experimental techniques. It was evidenced that a stagnation point forms on the frontal face of the obstacle that initiates a driving force to run the fluid underneath of the obstacle. It also is a cause of creating a circulation zone downstream to the insert. The feature is common to all boundary layers disturbed by an obstacle and is also reported by kahrom [10] and Sarkar [11].

The occurrence of the stagnation point and a jet are inevitable consequences of inserting an obstacle into a boundary layer. The effect brought by these flow features can suggest that the configuration of obstacle shape and its distance from the wall can affects on near wall flow structure and therefore on optimal of heat transfer enhancement from the neighboring wall. Depending on the shape and the distance of the obstacle from the wall, it would be possible to gain better heat transfer which has been ignored in the reviewed literature. Hence, the objective of present research is to group best combination of quad's faces and its distance from the wall to perform the best enhancement of heat transfer from neighboring flat plate.

2. PROBLEM DESCRIPTION AND PRECAUTION

In developing of a boundary layer, the laminar boundary layer is subject to strong molecular shears, killing the circulating flows and turbulent eddies. Therefore, the laminar boundary is eliminated from present study and the turbulent boundary layer remains for further examination. A turbulent boundary layer of about $Re_x = 10^6$is then selected for present investigation. A flat plate with 2m height and flow of air with a velocity of 14 m/s parallel to the plate are assumed. At $x = 1.4\,m$ from the leading edge, $Re_x$is 10^6 and the rest of the flat plate remains long enough to allow the boundary layer to handle the augmentation and explore the effect on the heat transfer.

The temperature difference of 50 ℃ is maintained between the flow stream and the flat plate. If assuming the ambient temperature of about 20 ℃, as normally is, the wall temperature is fixed at 70 ℃.

To keep the obstacle deep inside the boundary layer, the frontal edge of the quad is kept about 8mm and other faces are calculated by employing GA reasoning.

Therefore, the stream of air flows at 14 *m/s* parallel to a flat plate. The flat plate is isothermal and is kept at constant temperature at 70^0C. The temperature difference between the plate and the main stream maintained constant at 50^0C. The boundary layer is then disturbed by a quadrilateral bar at a point where the local Reynolds number based on the stream-wise distance from the plate leading edge is *1.6E* + 06. Later, the problem is focused on design and manipulation of a quad and its distance from the neighboring flat plate aiming to maximize the overall heat transfer coefficient from the plate. The distance of quadrilateral from the wall is changed by steps for each of quadrilaterals which are accepted for examination. The quad shape manipulation is decided as a consequential decision making advised by the aid of the genetic algorithm. For each case, i.e. the quad shape and its distance from the plate, the effect on heat transfer coefficient over the affected area is evaluated. Here, the affected area is defined to be a distance along the flat plate over which the wall heat transfer coefficient differs by more than $\mp 5\%$ from its identical value for an undisturbed flow. A schematic diagram of the problem is shown in Figure 1.

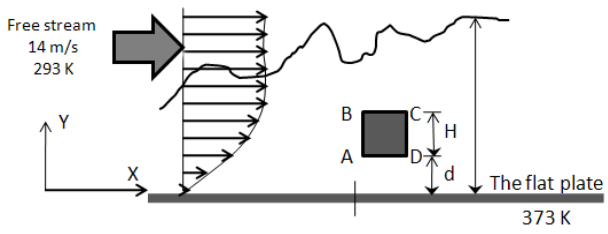

Figure 1. Schematic diagram of the flow arrangement

Despite emphasizes is made in choosing a quadrilateral insert, one can refer to the unique advantage accompanied by flow features around a quad. It provides definite points of flow separation. Unlike a blunt body, the flow separation points are fixed at rear sharp edges of the quad and the positioning are independent of the obstacle Reynolds number. Therefore, separation points can be designed, somehow, irrelevant to optimization of other quad faces.

3. GOVERNING EQUATIONS

Based on the small amount of flow velocity and temperature changes, the airflow is considered to be incompressible. The flow assumed to be turbulent with small viscous dissipation. Then the Reynolds Averaged Navier-Stokes equations (RANS) read as:
The continuity equation:

$$\frac{\partial}{\partial x_i}(\rho u_i) = 0 \qquad (1)$$

The Momentum equation for incompressible flow with no dilatation term on the right hand side is:

$$\frac{\partial}{\partial x_i}(\rho u_i u_j) = -\frac{\partial p}{\partial x_j} + \frac{\partial}{\partial x_i}\left[\mu\left(\frac{\partial u_i}{\partial x_j} + \frac{\partial u_j}{\partial x_i}\right)\right] + \frac{\partial}{\partial x_i}\left(-\rho\overline{\acute{u}_i\acute{u}_j}\right) \qquad (2)$$

in which,

$$-\rho\overline{\acute{u}_i\acute{u}_j} = \mu_t\left(\frac{\partial u_i}{\partial x_j} + \frac{\partial u_j}{\partial x_i}\right) \qquad (3)$$

The total shear stress is thus:

$$\tau_{tot} = \mu\frac{\partial u_i}{\partial x_j} - \rho\overline{\acute{u}_i\acute{u}_j} \qquad (4)$$

And the energy equation:

$$\rho\, u_j\frac{\partial T}{\partial x_j} = \frac{\partial}{\partial x_j}\left[\frac{\mu}{Pr}\frac{\partial T}{\partial x_j} - \rho\overline{T' u_j'}\right] - R_T \qquad (5)$$

For time averaged quantities, the boundary conditions are the same as for laminar flows, i.e. no slip condition for velocity components at fixed walls. As the turbulent fluctuations vanish at the wall, the shear stresses are produced only by molecular viscosity at the walls. We further assume that the wall temperature exhibits no fluctuation. Therefore, the shear stress equation $\tau = \mu(\frac{\partial u}{\partial y})$ and heat flux $q = -\lambda(\frac{\partial T}{\partial y})$ are still valid quantities at the wall, as is the pressure [1]. Equations 2 to 5 still have further unknowns, the Reynols stresses, the turbulent heat transfer $(\overrightarrow{\acute{v}\acute{T}})$ and the turbulent dissipation $\rho\tilde{\varepsilon}$. To close above mentioned equations, one of the eddy viscosity turbulence models is employed.

Zhang et al. [12], made an evaluation on turbulence models. Zero equation, $RNG\ k-\varepsilon$, $SST\ k-\omega, LRN-LS, v2f-daw, RSM, DES$ and LES are examined. Models were employed for many variety physical environments, such as natural convection in a tall cavity, forced convection in a room with partitions, mixed convection in a square cavity and strong buoyant flow. Comparison between numerical results and experimental measurements showed that: 1) the $RNG\ k-\varepsilon$ was even better than LES in prediction of mean temperature distribution 2) It was also equally good as LES in predicting average velocity of the flow and 3) It was better than LES in evaluation of turbulence distribution.

Comparing computer time consumption based on 0-equation model, the $RNG\ k-\varepsilon$ and $SST\ k-\omega$ consume 2-4 times, $LRN-LS$ and $v2f-daw$ consume 4-8 times, RSM 10-20 times, finally the DES and LES 100-1000 times. Zhang concluded that amongst the RANS models, v2f and RNG have the best overall performance in terms of accuracy, computing efficiency and robustness.

In present work some curious limitations must be regarded in choosing closure equations. For 2000 program runs to be continually and safely conducted, the total computer time consumption, stability of calculation and solution accuracy are all of crucial importance. $RNG\ k-\varepsilon$ carry advantage of even lower than v2f convergence time per run, together with good accuracy on predicting temperature and velocity distribution in the flow field, as described by Zhang, [12]. Moreover, authors of this paper have experience of using $RNG\ k-\varepsilon$ as closing equations. They have used the model in the present investigation.

As was accepted in the standard $k-\epsilon$ model, the transport equations for the kinetic energy, k, is, [13]:

$$\rho u_j \frac{\partial k}{\partial x_j} = \frac{\partial}{\partial x_j}\left[\left(\mu + \frac{\mu_t}{\sigma_k}\right)\frac{\partial k}{\partial x_j}\right] + P_k - \rho\epsilon \quad (6)$$

As the k equation is common to all 2-equations EVMs, the dissipation equation for RNG model reads as:

$$u_j \frac{\partial \epsilon}{\partial x_j} = C_{\epsilon 1}\frac{\epsilon}{k}\nu_{eddy}\, s^2 - C_{\epsilon 2}\frac{\epsilon^2}{k} - R + \nabla\alpha\nu_T\,\nabla\epsilon \quad (7)$$

where, $\nu_{eddy} = C_\mu \frac{k^2}{\epsilon}$, $C_\mu = 0.0845$, $\nu_T = \nu_{eddy} + \nu_{mol}$,and

$$R = \frac{C_\mu \eta^3 (1-\eta/\eta_0)}{1+\beta\,\eta^3}\,\frac{\epsilon^2}{k} \quad (8)$$

Here, $\beta = 0.012$, $\eta_0 = 4.38$ are constants and $\eta = S\,k/\epsilon$ is defined when $S^2 = 2S_{ij}S_{ij}$ and the magnitude of the strain rate is:

$$S_{ij} = (\partial u_i/\partial x_j + \partial u_j/\partial x_i)/2 \quad (9)$$

The RNG theory evaluates the constants $C_{\epsilon 1} = 1.42$, $C_{\epsilon 2} = 1.68$, and $\alpha = 1.39$. The inverse turbulent Prandtl number, α, differs from that of the standard $k-\epsilon$ model, in which $\alpha = 1$. Indeed, the value of α derived by the RNG scalar heat transfer relation is:

$$\left|\frac{\alpha-1.3929}{\alpha_0-1.3929}\right|^{0.6321}\left|\frac{\alpha+2.3929}{\alpha_0+2.3929}\right|^{0.3679} = \frac{\alpha_0}{\nu_T} \quad (10)$$

For the heat transfer problems α_0 refers to the molecular inverse Prandtl number. In regions of small η, the value of R tends to somewhat increasing the eddy viscosity and in regions of very large η, where strong anisotropy exists, R can becomes negative and it reduces the eddy viscosity even more. This feature of the RNG model holds the most attraction in that it gives better performance in anisotropic large-scale eddies [14]. While the standard $k-\varepsilon$ model is a high Reynolds number model, the RNG theory provides an analytically-derived differential formula for effective viscosity that accounts for low Reynolds number effects as well. The efficacious use of this feature, however, depends on appropriate treatment of the near-wall refinement and location of the first grid point to be inside the sub-layer. The turbulent heat flux, $-\rho\overline{T'u_j'}$, in Equation 5 is then obtained according to the simple gradient diffusion:

$$-\rho\overline{T'u_j'} = \frac{\mu_t}{\sigma_t}\left(\frac{\partial T}{\partial x_j}\right) \quad (11)$$

where, σ_t is the turbulent Prandtl number which its value is given as 0.85.

The numerical method to solve the equations is based on the control-volume formulation. The physical domain is divided into control volumes. Each control volume is associated with a discrete point at which dependent variables, such as velocity, pressure and temperature, are to be calculated. Discretization equations are derived by integrating the Equations 1 to 7 over these control volumes. Figure 2 shows a sample rectangular computational domain subdivided into such control volumes. In this figure, the dashed surfaces denote the control volume.

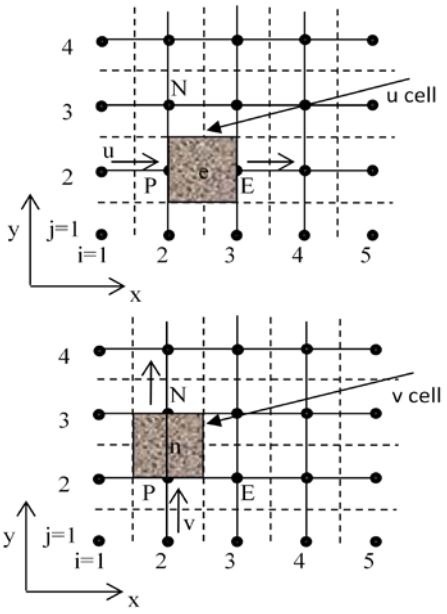

Figure 2. Momentum control volume.

The two sides of the control volume on grid e are the faces to count for upstream momentum and the component of velocity u_e at e. The top and bottom surfaces are similarly employed for the calculation of component v_n of the velocity.

Staggered grid arrangements are used on which the nodes for velocity components are located at mid points on the cell sides. In this case, pressure and temperature are at the cell centre.

A first order implicit scheme is employed for discretising the time derivatives. The pressure is

linked between the continuity and momentum equations. Finally, by calculating the density and velocity components, the energy equation is solved.

4. GRID GENERATION AND CODE VERIFICATION

Grid point's distributions in a computational domain are assumed to be non-uniform. Unlike a single flow field examination that is the subject of much of research works, the present work comprises 1,600 different compositions of a quad and a flat plate boundary layer that must be re-meshed and resolved sequentially. It is difficult to address a precise mesh organization. Here, to achieve the best use of turbulence models, the laminar sub-layer must be touched by the model. In other words, at least one grid point must be located inside the sub-layer. Therefore, the strategy in each re-meshing is to locate the first grid point on the solid walls, along with the flat plate and surfaces of the quad. Then, the next grid point is located at a distance of not more than $y_2^+ - y_1^+ < 5$, where $y^+ = yu_\tau/v$ is near-wall coordinates, u_τ and v are the shear velocity and kinematic viscosity respectively. If the second node is placed at $y_2 = 0.1\,mm$ from the wall, experience from this work shows that the mentioned criteria will be reached. Node number 3 and so on are then positioned by stretching the distance between nodes by a factor of s. The same reasoning applies to nodes in the x direction. The finest meshing is, therefore, found in the gap between the quad and the flat plate.

The same strategy is followed for meshing of the computational domain for each new geometrical configuration.

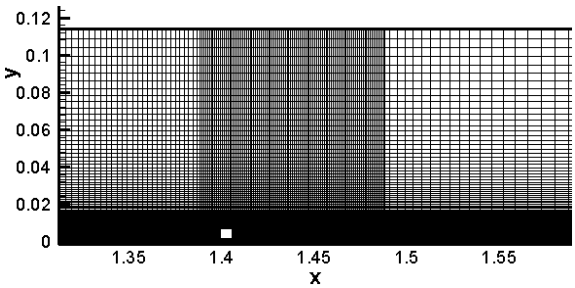

Figure 3. Sample meshing for a rectangular obstacle near a flat plate.

A no-slip condition is imposed on the flat plate and surfaces of the quad. The height of flow over the flat plate is chosen so that it is large enough to minimize the influence of flow blockage due to growth and disturbances imposed by the boundary layer.

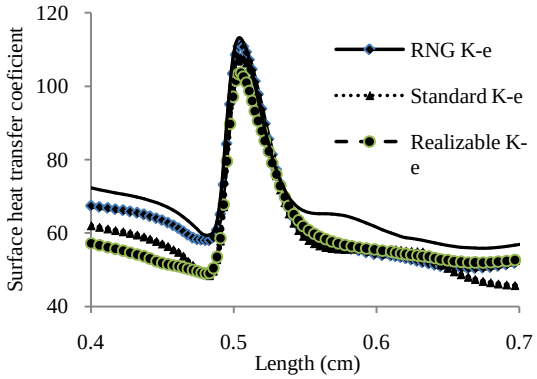

Figure 4. Turbulence models in prediction of enhanced HTC on a flat plate

Along with reporting the adequacy of meshing strategy, the author of this study, in reference [10], tests the accuracy of the computer code, the validity of the final solution, and grid dependency of the code solution for the boundary layer that was disturbed by an insert. Nevertheless, to assure the validity of the present numerical code, hot wire anemometry is performed in a wind tunnel. Similar flow field and condition, as described in section 2, is imposed. A square rod, with a cross section of $8\,mm \times 8\,mm$, is placed at a distance $D = 8\,mm$ from the flat plate, inside the turbulent boundary layer of the flat plate where $Re_x = 1.63E + 06$ and the average velocity measured at downstream to the rod [15]. The comparison between the solution of the present code and measurements at a distance of $\frac{x}{c} = \frac{5}{8}$ is shown in Figure 5, x is the distance from the rear stagnation point on the quad and c is the length of the quad. As the figure shows, strong agreement exists between the experimental and numerical solutions. The figure compares the solutions for three cases of mesh generations with assuming the stretching factor being $s = 1.08$ (grids 410*167), $s = 1.1$ (grids 390*155), and $s = 1.12$ (grids 370*140). Optimal agreement at s=1.08 is reached; the meshing strategy accepted and is employed throughout the present study.

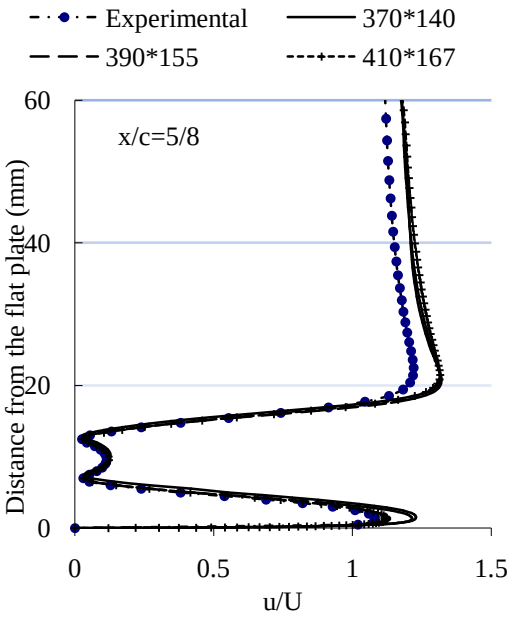

Figure 5. Comparison of mean velocity profiles with measured data

Another comparison between the present code and the solution of the Fluent code is made by comparing solutions for the same case as explained above. Results are presented in Figure 6. This figure also shows the estimation of the code for HTC compared with the empirical law for a single flat plate. In both cases the code is in satisfactory agreement with referenced data.

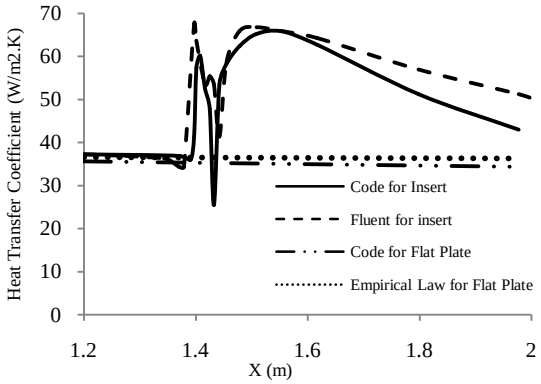

Figure 6. Comparison between the present program and the Fluent code and empirical law for a flat plate

5. OPTIMIZATION TECHNIQUE

GA is an accepted technique in optimization of problems with multiple depending functions. McCormack [16] optimized the suction side pressure distribution over a flat plate to delay separation and to minimize drag force. In another study design of a plane was optimized by GA to achieve best maximum lift and minimal drag forces [17].

Herein, the GA is employed as an optimization tool to maximize the overall heat transfer coefficient. The average heat transfer coefficient is defined by Equation 12 and it is applied to individual profiles through the optimization.

$$\overline{h_c} = \frac{1}{\Delta x}\int_{x_1}^{x_2} h_{cx}\, dx \qquad (12)$$

where,

$$h_{cx} = -k\left(\frac{T_{i,2} - T_w}{y_{i,2}}\right) \Big/ (T_w - T_\infty) \qquad (13)$$

The eight geometrical coordinates of the quadrilateral object in Figure 1 are defined as the limits of fitness functions. Further, to secure the quad edges to stand within a certain logical constraint, geometrical limitations are imposed. In Tables 1 and 2, limits for the coordinates A, B, C and D are described.

TABLE 1. Limits of the geometrical features in GA

Parameter	Geometrical limits
Point A	$1.4(m) \le x_a \le 1.41(m)$ $1.4(mm) \le y_a \le 9.8(mm)$
Point B	$1.4(m) \le x_b \le 1.414(m)$ $2.2(mm) \le y_b \le 12(mm)$
Point C	$1.406(m) \le x_c \le 1.42(m)$ $2.2(mm) \le y_c \le 12(mm)$
Point D	$1.406(m) \le x_d \le 1.42(m)$ $1.4(mm) \le y_d \le 9.8(mm)$

TABLE 2. constraints of the geometrical features in GA

Condition	Geometrical constraint
1	$x_a < x_d$
2	$x_b < x_c$
3	$y_a < y_b, y_a < y_c$
4	$y_a = y_d$

Based on results for some sample runs of the code, the initial population is chosen. This selective start of computation helps to improve general performance of GA technique. Additionally, the design variables and the fitness functions are saved at the end of each program run. Then, new geometrical variables are checked with the database before being processed by the code to debar recapitulation. The optimization process and how the GA is coupled with the flow solver is shown as a flowchart in Figure 7.

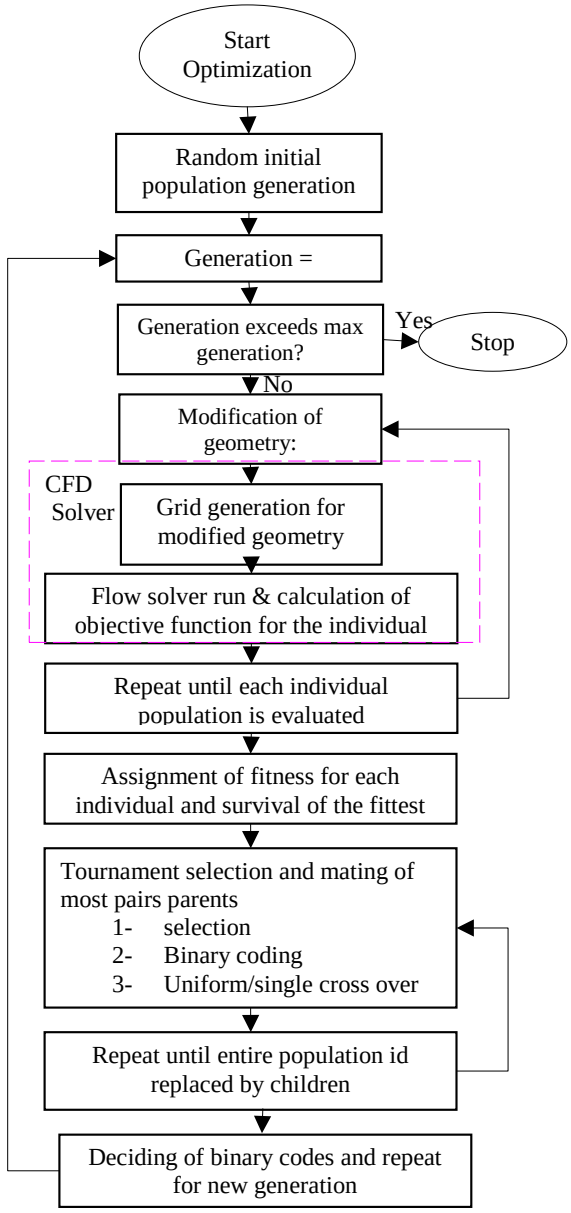

Figure 7. Flowchart of optimization procedure

6. RESULTS

During the solution process, from each sample of generation, optimized solution is taken for study of flow behavior around the obstacle. Three zones of significant effect on flow behavior are illustrious for all samples. A stagnation point on the frontal area, a jet between obstacle and the flat plate and finally a vortex zone trailed after the quad. This interacting feature will be discussed next. More detail of the optimization technique is discussed by kahrom et al. [18].

Single objective genetic algorithm is applied to introduce the optimal coordinates of a quad according to the aforementioned geometrical constraints. The best design is one that yields the maximum average heat transfer coefficient over the affected area compared to the rest of the populations in that generation. Parameters affecting the optimization are coordinates of quad vertices, the number of population in each generation and the method by which population in each generation is to be calculated, Table 3.

In the authors experience, mutation rates in the range of 0.006 to 0.011 lead to stable, better and faster convergence to final results. Herein, the probability of mutation is considered to be 0.009 while the probability of cross-over rate is assumed to be 0.88.

TABLE 3. Parameters used in single objective GA optimization of heat transfer coefficient.

Number of population	*20*	Selection method	*Ranking*
Initial population generation method	*Random*	Mutation method	*Structured*
Total number of generations	*100*	Crossover method	*Two-point*
Stop criterion	*100^{th} generation*		

The successful round of optimization took about 500 hours on a system with a 2.8GHz processor and 4GB RAM. The best and average values of the fitness function are shown in Figure 8 for each generation. After the 18^{th} generation, the minimal skin friction coefficient remains unchanged. However, the average value of the fitness function improves to achieve the maximal

heat transfer coefficient. The geometrical features of the optimal layout are presented in Table 4.

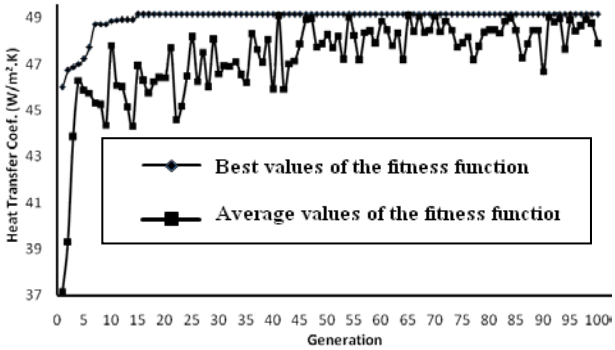

Figure 8. Variation of the fitness function through different generations

TABLE 4. Coordinates of the suggested optimal profile for the maximum overall heat transfer coefficient

	Point A	Point B	Point C	Point D
x	$1.405\,m$	$1.405\,m$	$1.407\,m$	$1.42\,m$
y	$1.4\,mm$	$12\,mm$	$2.2\,mm$	$1.4\,mm$

A sample variation of the heat transfer coefficients along the wall in the affected area compared to the results of a single flat plate is plotted in Figure 9a. Fluctuations of heat transfer coefficient are due to strong convection caused by the velocity gradients near the wall and the recirculation zone behind the obstacle. Streamlines around the optimal geometry are drawn in Figure 7. The figure shows, as a consequence of presence of a fluid jet, the boundary layer deforms underneath of the obstacle, and heat transfer increases accordingly.

General behavior of the Local Heat Transfer Coefficient (LHTC) curve for a flat plate affected by an obstacle, is typically shown in Figures 9a and 9b. The curve confirmed the outcomes frequently were concluded from numerical and experimental data which was generated by author of this paper and other research workers in this subject [19] and [20]. The curve presents 5 distinct zones. Zone (I) is beginning of a slowdown of flow due to the presence of a stagnation point on the frontal area of the quad. Pressure at this point increases and

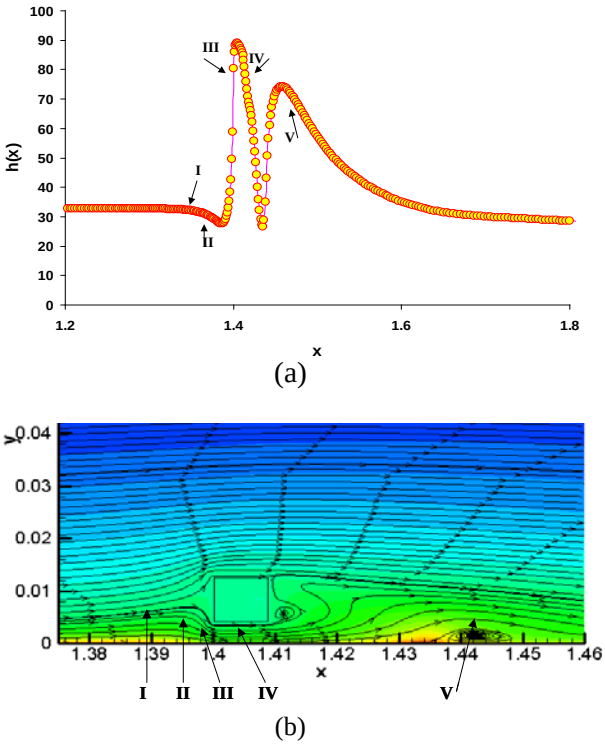

Figure 9. Typical effect of obstacle to enhance heat transfer from neighboring flat plate, (a) variation of LHTC, (b) streamlines showing effected flow, x in meters from plate leading edge

generates motive force to drive the flow through the gap which is formed underneath of the obstacle. At the zone (II) flow decelerates and divides into two sides. Slow down of flow causes a bit reduction in LHTC. One part of flow then accelerates towards the starting point of the gap, zone (III). In this zone LHTC rises sharply up to the gap entrance. After this zone, inside the gap a new boundary layer starts to grow up, along which LHTC decreases again to a minimum. Outside the gap, at rear side of the obstacle and upon exiting jet, a small vortex may form. This vortex is always a cause of slow down of flow and dropdown in LHTC, Zone (IV). Finally, leaving jet forms another vortex followed by low thickness boundary layer along a quiet wide range which causes the dominate contribution to overall heat transfer, zone (V). Not normally this area giving the highest LHTC, but its effect on a long area of the plate is deterministic throughout present work. Contribution of each zone to heat transfer is a

function of obstacle geometry and its distance from the flat plate. The first vortex occurs due to shear stress resulting from jet flow leaving the gap. Then, the jet detaches from the flat plate, i.e. another vortex forms in-between. This second vortex has widest contribution to heat transfer enhancement and must be watched closely when obstacle regeneration is considered (Figure 9b).

While frontal stagnation point generates the driving force to run a jet through the gap beneath of the obstacle, the rear face accommodates downstream vortices to form and expand over the flat plate, Figures, 9 and 10. In the following example, a comparison between some populations of a generation, at variety distances from the flat plate, is made according to Figure 10. The heat transfer and friction coefficient resulting from obstacle shape and its distance from the wall is demonstrated. A quad of trapezoidal shape is modified by changing the size of frontal, the rear and lower faces together with the obstacle distance from the flat plate.

Figure 10a, shows important constants of the quad and the angle α which shall be tailored during the test. Figures 10b, c and d are solutions of computer program for flow around the trapezoidal for the $\alpha = 25, 50, 75$ respectably. The effect on the flow features, heat and friction coefficients are presented in Figures 10 e to h. Variation of heat transfer coefficients for each case is presented in Figure 10e. Since the overall heat transfer is more lucid than its local values, in Figure 10f the comparative averaged values over the affected area for 3 cases are shown. Similar to HTC, the local and averaged values of friction coefficients are of decisive value and are presented in Figures 10g and h.

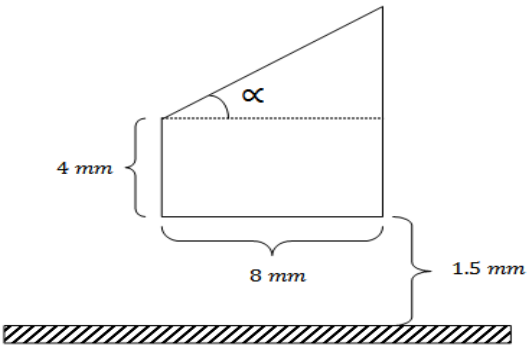

(a)

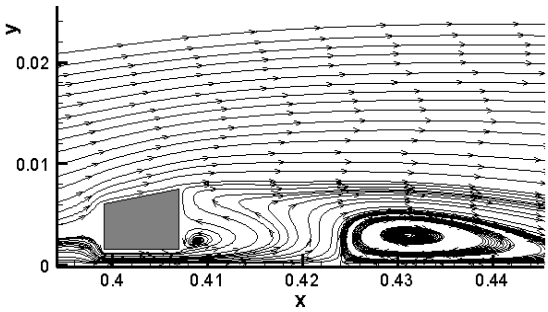

(b)

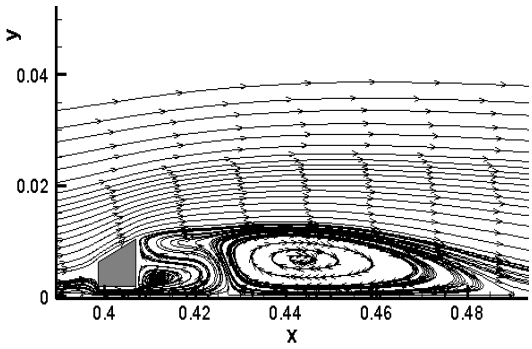

(c)

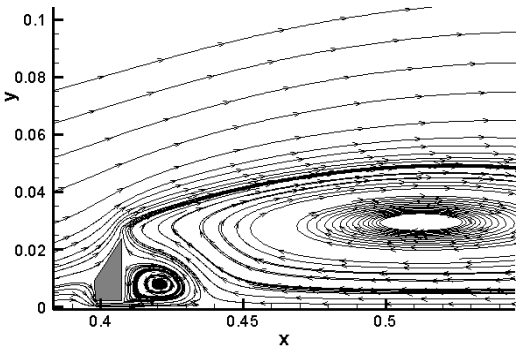

(d)

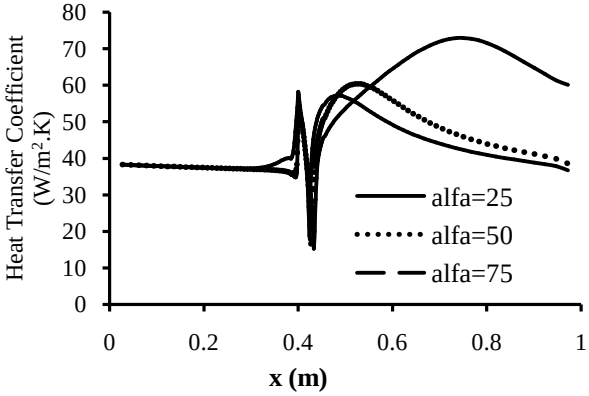

(e)

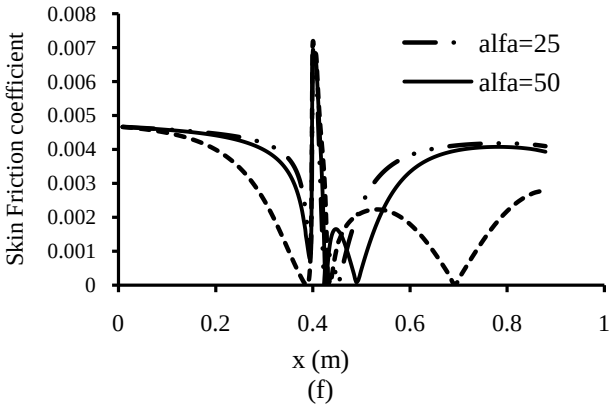

(f)

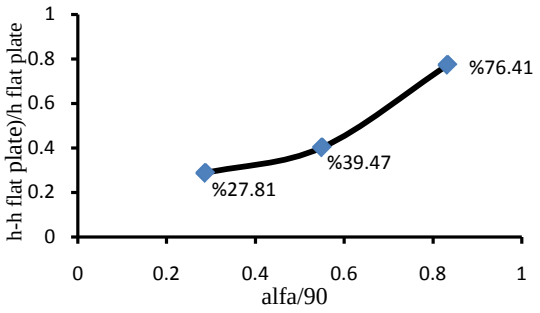

(g)

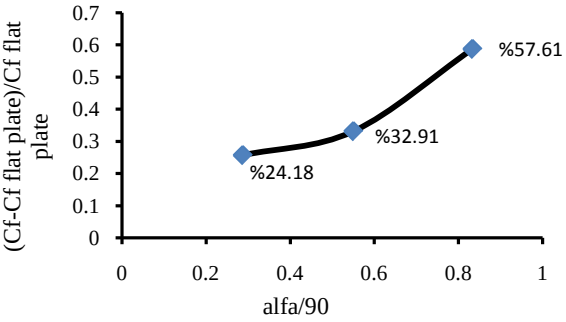

(h)

Figure 10. Examples of quads disturbing a boundary layer over a flat plate.

Solutions for 100 generations, with 20 populations in each generation are performed. Indeed, 2000 cases are solved and results are compared to find the best quad for enhanced heat transfer while keeping lowest friction coefficient. Finally, the optimal shape is caught; a quad, having an L shape, according to Figure 11. So, the heat transfer variation over a long surface of a flat plate is plotted in Figure 12.

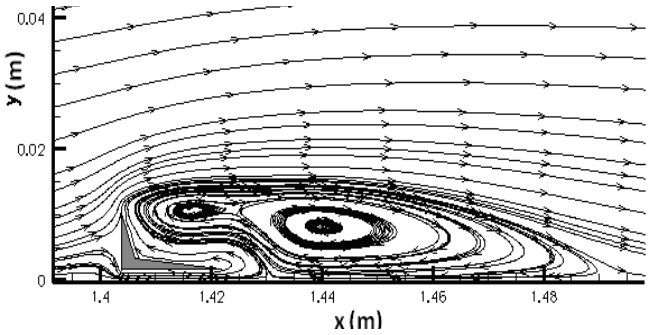

Figure 11. Streamlines around the optimal geometry for the highest heat transfer coefficient

The coordinates of four vertices of the optimal quad are presented in Table 4. Equation 14 is used as an experimental tool to measure the enhancement, Figure 12. Good agreement between numerical solution and empirical law for single flat plate presented. When obstacle effect is encountered, enhancement effect is revealed by comparison. The experiment prediction for overall heat transfer coefficient is about 35.8 $W/m^2.K$, if a boundary is not perturbed. The value of averaged heat flux achieved 54.2 $W/m^2.K$, when the optimal obstacle is inserted to the boundary layer for identically similar area of the flat plate. Comparing these values shows an increase of 51.17% of the overall heat transfer coefficient as a result of adopting the proposed geometry.

$$Nu_x = \frac{h_x x}{k_f} = 0.0296\,\mathrm{Re}^{4/5}\,\mathrm{Pr}^{1/3} \qquad (14)$$

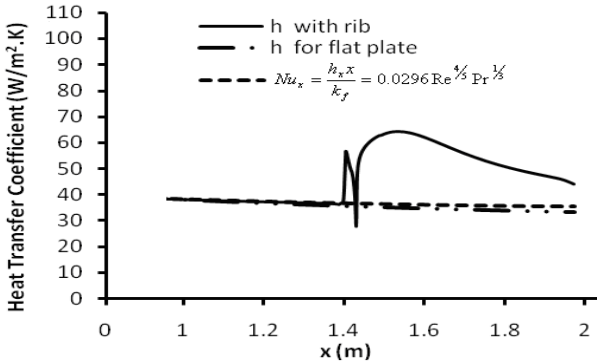

Figure 12. Variation of heat transfer coefficient along the flat plate, in presence and in absence of the optimal obstacle

7. CONCLUSION

Complexity of flow behind an obstacle and the number of varieties of parameters involved makes the optimization of flow structure a difficult task. The GA technique together with the modified (Teach-t) code was applied to investigate the geometry of the optimal insert's shape. The optimization was done through the single objective algorithm both for the heat transfer and skin friction coefficients. The numerical results indicate that the overall heat transfer coefficient is dependent to the height of the obstacle and there is an inverse relation with the obstacle distance from the plate. The jet formed beneath of the manipulator increases the heat transfer coefficient and has an adverse effect on the wall skin friction by wiping out the boundary layer. This optimized object enhances the overall heat transfer by about 51% when averaging is taken over the affected area. Considering jet and circulation zone downstream to the blunt body as the main sources of enhancement, the circulation zone has the most contribution on enhancement. While the maximum was devoted to the affect of jet, wider range of the enhancement was due to the affect of recirculation zone.

8. REFERENCES

1. Schlichting H. and Gersten K., "Boundary layer theory", ISBN 3-540-66270-7, Springer, (2000).
2. Balaras, C., "A review of augmentation techniques for heat transfer surfaces in single phase heat exchangers", ***Journal of Energy***, Vol. 10, (1990), 899-906.
3. Baskaran, V. and Bradshaw, P., "Effect of bluff body wakes on skin friction and ssurface heat transfer in a turbulent boundary layer", ***Journal of Wind Engineering and Industrial Aerodynamics***, Vol. 49, No. (1-3), (1993), 269-278.
4. Joardar, A. and Jacobi, A.M., "Heat transfer enhancement by winglet-type vortex generator arrays in compact plain-fin-and-tube heat exchangers", ***International Journal of Refrigeration,*** Vol. 31, (2008), 87-97.
5. Kawaguchi, Y., Suzuki, K. and Sato, T., "Heat Transfer Promotion with a Cylinder Array Located Near the Wall", ***International Journal of Heat and Fluid Flow***, Vol. 6, No. 4, (1985), 249-255.
6. Marumo, E., Suzuki, K. and Sato, T., "Turbulent heat transfer in a flat plate boundary layer disturbed by a cylinder", ***International Journal of Heat and Fluid Flow***, Vol. 6, No. 4, (1985), 241-248.
7. Suzuki, H., Suzuki, K. and Sato, T., "Dissimilarity between heat and momentum transfer in a turbulent boundary layer disturbed by a cylinder", ***International Journal of Heat and Mass Transfer***, Vol. 31, No. 2, (1988), 259-265.
8. De Souza, F., Delville, J., Lewalle, J. and Bonnet, J.P., "Large scale coherent structures in a turbulent boundary layer interacting with a cylinder wake", ***Experimental Thermal and Fluid Science***, Vol. 19, (1999), 204-213.
9. Inaoka, K., Yamamoto, J. and Suzuki, K., "Dissimilarity between heat transfer and momentum transfer in a disturbed turbulent boundary layer with insertion of a rod-modelling and numerical simulation", ***International Journal of Heat and Fluid Flow***, Vol. 20, No. 3, (1999), 290-301.
10. Kahrom, M., Farievar, S. and Haidari, A., "The effect of square splittered and unsplittered rods on flat plate heat transfer", ***IJE Transactions A: Basics***, Vol. 20, (2007), 83-94.
11. Sarkar, S. and Sarkar, Sudi., "Vortex dynamics of a cylinder wake in proximity to a wall", ***Journal of Fluids and Structures,*** Vol. 26, (2010), 19-40.
12. Zhang, Z., Zhang, W., Zhai, Z. and Chen, Q., "Evaluation of various turbulence models in predicting airflow and turbulence in enclosed environments by CFD: Part-2: comparison with experimental data from literature", ***HVAC&R Research***, Vol. 13, No. 6, (2007).
13. Davidson, L., "An introduction to turbulence models, publication", 97/2, Department of Thermo and Fluid Dynamics, Chalmers University of Technology, (2003).
14. Gatski, T.B., Hussaini, M.Y. and Lumley, J.L., "Simulation and modeling of turbulent flows", ICASE/LaRc Series in Computational Science and Engineering, Oxford University Press, Inc., ISBN 0-19-510643-1, (1996).
15. Kahrom, M., Khoshnewis, A.B. and Bani Hashemi, H., "Hot Wire Anemometry in the wake of a trapezoidal in the vicinity of a falt plate", Report No. 40258, Faculty of Engineering, Ferdowsi University of Mashhad, (2009).
16. McCormack, W., Tutty O.R. and Rogers E., "Stochastic optimization based control of boundary layer transition", ***Control Engineering Practice***, Vol. 10, (2002), 243-260.
17. Ng, T.T.H. and Leng, G.S.B., "Application of genetic algorithms to conceptual design of a micro-air vehicle", ***Engineering Application of Artificial Intelligence***, Vol. 15, (2002), 439-445.
18. Kahrom, M., Haghparast, P. and Javadi, M., "Optimization of heat transfer enhancement of a Flat Plate Based on Pareto Genetic Algorithm", ***International Journal of Engineering***, Vol. 23, (2010), 175-187.
19. Mahir, N., "Three-Dimensional flow around a square cylinder near a wall", ***Journal of Ocean Engineering***, Vol. 36. (2009), 357-367.
20. Bhattacharyya, S. and Maiti, D.K., "Shear flow past a square cylinder near a wall", ***International Journal of Engineering Science***, Vol. 42. (2004), 2119-2134.